An evaluation of the microstructure and microhardness in an Al-Zn-Mg alloy processed by ECAP and post-ECAP heat treatments

Mohamed A. Afifi[a], Ying Chun Wang[a,b] *, Xingwang Cheng[a,b], Shukui Li[a,b], Terence G. Langdon[c]

[a]School of Materials Science and Engineering, Beijing Institute of Technology, Beijing 100081, China
[b]National Key Laboratory of Science and Technology on Materials under Shock and Impact, Beijing 100081, China
[c]Materials Research Group, Department of Mechanical Engineering, University of Southampton, Southampton SO17 1BJ, UK
*Corresponding author: Ying Chun Wang, e-mail: wangyc@bit.edu.cn

Keywords: Al-Zn-Mg alloy; equal-channel angular pressing (ECAP); post-ECAP heat treatment; microhardness; precipitates

Abstract

An investigation was conducted to examine microstructure evolution and microhardness variations in a peak-aged Al-Zn-Mg alloy after equal-channel angular pressing (ECAP) for 1 to 8 passes followed by heat treatments at temperatures of 393 to 473 K for times from 5 to 20 h. The results show that ECAP processing hardens the alloy and the hardness increases with each pass due to grain refinement, the formation of large numbers of fine precipitates and the introduction of a high dislocation density. Post-ECAP annealing at 393 K up to 20 h after 1 and 4 passes of ECAP leads to a further increase in microhardness and this increase is substantial for an annealing time of 20 h after 1 pass due primarily to the extensive formation of a nano-sized η′ phase. After ECAP for 8 passes, a post-ECAP annealing at 393 K for 5 h or more leads to softening due to the occurrence of recrystallization and the transformation of fine η′ to coarse η. The results show that post-ECAP anneals at the higher temperatures of 423 or 473 K are not capable of producing high hardness values.

1. Introduction

Al-Zn-Mg alloys are widely used in aerospace and automobile applications because of their high strength-to-weight ratio [1,2]. In this series of aluminum-based alloys, the conventional strengthening methods are solid solution and peak aging treatments which form fine and uniformly distributed precipitates within the Al matrix [3,4]. The presence of large numbers of fine coherent G.P. zones and semi-coherent η' phase is responsible for the strengthening of materials after the aging treatment [5, 6]. Nevertheless, there is considerable interest in further improving the mechanical behavior of these alloys.

Processing by severe plastic deformation (SPD), as in equal-channel angular pressing (ECAP), is an effective procedure for producing metals and alloys having ultrafine-grained (UFG) structures [7-11]. The mechanical properties of Al-Zn-Mg alloys can be enhanced by a combination of strain hardening, grain boundary strengthening and precipitation hardening during ECAP processing and this will promote the use of these materials in industrial applications [12-16]. For example, the hardness of a 7075 Al alloy was higher by ~70 Hv after 4 passes of ECAP than in the annealed alloy [17].

Several reports suggest that even further improvements in the mechanical properties may be achieved in the Al-Zn-Mg alloys through the use of post-ECAP heat treatments [13,14,16,18-20]. Thus, a post-ECAP heat treatment at 393 K for 16 h enhanced the ultimate strength of a 7050 Al alloy by ~150 MPa by comparison with the alloy before ECAP [14] and this strengthening was primarily due to the fine precipitates produced during the post-ECAP heat treatment. In other studies, significant increases in hardness were achieved by post-ECAP heat treatments of an Al-7075 alloy containing a scandium addition [18] and of an Al-6061 alloy [19].

From an examination of these earlier experimental results, it is reasonable to conclude that improved mechanical properties may be achieved in Al-Zn-Mg alloys through the use of appropriate ECAP processing followed by the application of optimal heat treatments. Nevertheless, only limited data are available at present to provide information on the precise influence of various post-ECAP heat treatments on microstructural parameters such as the evolution of a refined grain size, the variation of the microhardness and the strengthening associated with selected Al-Zn-Mg alloys [21-23].§ Furthermore, in order to extend the available

---

§It is important to note that in an earlier report [21] the composition of the alloy was given as Al-4.6 Zn-2.58 Mg-0.35 Mn-0.2 Cr as supplied on purchase from the manufacturer. Later, with the identification of some precipitates containing Cu, the composition was carefully measured as Al-4.53 Zn-2.52 Mg-0.35 Mn-0.2 Cr-0.11 Cu-0.1 Zr. This composition is reported in the present paper and the material is the same as in the earlier report.

---

information so that these Al-Zn-Mg alloys may be used in applications associated with high temperature environments, it is necessary also to evaluate the thermal stability of the alloys after processing by ECAP. Accordingly, the present investigation was initiated to provide a set of detailed results documenting the relationship between the microstructure and the microhardness of an Al-Zn-Mg alloy both after ECAP processing through different numbers of passes and after post-ECAP annealing for different times and over a range of different temperatures.

2. Experimental material and procedures

The experiments were conducted using an Al-Zn-Mg alloy having a composition, in wt%, of Al-4.53 Zn-2.52 Mg-0.35 Mn-0.2 Cr-0.11 Cu-0.1 Zr. The alloy was received after solid solution

processing at 743 K for 1 h and aging at 393 K for 24 h in a T6 treatment. Billets of the as-received material with diameters of 9.8 mm and lengths of 65 mm were processed through 1, 4 and 8 ECAP passes using a solid die having an internal channel angle of 90° and an outer arc of curvature of 20°. It can be shown that these angles lead to an imposed strain of ~1 on each separate passage through the die [24]. The ECAP processing was conducted at a temperature of 423 K using processing route B_c where the billet is rotated by 90° in the same sense about the longitudinal axis between each pass [25]. Following the ECAP processing, samples of the Al-Zn-Mg alloy were annealed at temperatures of 393, 423 or 473 K for periods of 5, 10, 15 or 20 h using a forced convection furnace and then cooled in air. For convenience, the processing using a combination of ECAP and subsequent heat treatment is henceforth designated post-ECAP HT.

The microhardness was measured using a Vickers hardness tester under an applied load of 50 kgf with a dwell time of 15 s. Samples with diameters of ~5 mm were cut from the centers of the transverse sections of the ECAP billets and they were then ground and polished prior to conducting the hardness testing. The average hardness values were obtained by averaging 10 separate hardness measurements for each testing condition.

Microstructural observations were performed using transmission electron microscopy (TEM) with an FEI Tecnai G2 F20 X-TWIN operating at 200 kV. For TEM characterization, thin foils of the materials were cut from the centers of the cross-sections of each billet on planes lying perpendicular to the pressing direction. The samples were then prepared by electro-polishing in an electrolyte of 8% perchloric acid and 92% ethanol at 248 K using a voltage of 22 V and a current of ~40 mA. After electro-polishing, the samples were further thinned by ion-milling using a Leica RES 101 at 3 kV under a current of 1 mA for 30 min in order to remove any possible contamination that may have been introduced by the electro-polishing. Using TEM, average

particle sizes were measured by calculating the mean of ~500 particles for each processing condition. The average grain sizes of the samples were measured from TEM images by counting more than 150 intercepts using the circular intercept method following the ASTM E112-12 standard.

3. Experimental results

3.1 Microhardness values after ECAP and post-ECAP heat treatments

The average Vickers microhardness values in the Al-Zn-Mg alloy are shown in Figure 1 after post-ECAP annealing at temperatures of 393, 423 and 473 K for times from 5 to 20 h for samples processed through (a) 1 pass, (b) 4 passes and (c) 8 passes of ECAP. In these illustrations, horizontal dashed lines are used to denote the measured hardness values of ~135 Hv in the initial as-received T6 condition and the values of ~150 Hv, ~153 Hv and ~168 Hv after 1, 4 and 8 ECAP passes, respectively. Thus, processing by ECAP effectively strengthens the alloy by comparison with the conventional T6 treatment.

It is readily apparent from inspection of Figure 1 that the effect on hardness of the post-ECAP HT depends both on the preliminary numbers of ECAP passes and the annealing parameters. For the sample processed through 1 pass of ECAP in Figure 1(a), post-ECAP annealing at 393 K leads to an increase in microhardness with increasing annealing time such that a maximum hardness of ~180 Hv was achieved after annealing for 20 h. The values after post-ECAP HT at 423 K are also slightly higher than after ECAP processing for annealing times of 5 and 10 h but after 15 and 20 h the values are similar to the ECAP condition. By contrast, post-ECAP annealing at 473 K for 5 to 20 h sharply reduces the hardness to values lower than in the T6 alloy.

For the 4 passes ECAP sample shown in Figure 1(b), post-ECAP HT at 393 K leads to higher hardness with a maximum value of ~167 Hv after annealing for 20 h. Although annealing at 423 and 473 K leads to slightly higher hardness than in the ECAP sample after 5 h, the hardness values are lower than in the ECAP alloy after longer annealing times. Annealing at 473 K again leads to low hardness values lying below the T6 sample for annealing times from 10 to 20 h.

Finally, in Figure 1(c) after 8 passes of ECAP, all annealing temperatures and all times lead to hardness values that are lower than in the sample processed only by ECAP. Thus, a post-anneal at 393 K is not satisfactory in the Al-Zn-Mg alloy after processing by ECAP through large numbers of passes.

In order to understand these hardness variations, it is necessary to conduct detailed microstructural characterizations of samples processed under the various experimental conditions. These results are described in the following sections.

3.2 Microstructures for post-ECAP annealing after 1 pass

For the as-received alloy, the initial grain size was ~1.3 μm and the material contained various precipitates: spherical G.P. zones of ~5 nm, plate-like η' of ~120 nm in size and some limited plate-like T ($Al_{20}Cu_2Mn_3$) and E ($Al_{18}Mg_3Cr_2$) [21]. It was shown earlier that processing by ECAP for 1 pass produced an elongated structure with a high dislocation density of ~3.5 × 10^{14} m^{-2} and with most of the η' precipitates refined to ~5 nm with a few precipitates maintaining a length of ~120 nm together with large numbers of G.P. zones having sizes of ~4 nm [21].

Observations by TEM after ECAP for 1 pass and post-ECAP annealing at 393 K for 5 h revealed dislocation recovery as shown in Figure 2 (a). Increasing the annealing time to 20 h gave a reasonably equiaxed dislocation cell structure as in Figure 2(d). For post-ECAP anneals at 423

K, a high dislocation density was visible after 5 h but the density decreased after 20 h as shown in Figures 2(b) and (e). Finally, there was evidence for the advent of recrystallization after annealing at 473 K and some recrystallized grains are visible after 5 h in Figure 2(c) whereas after 20 h there were equiaxed grains with a size of ~1 μm and a relatively low dislocation density in Figure 2(f) suggesting that recrystallization was complete.

TEM images for the same experimental conditions are given in Figure 3 and these show fine spherical precipitates with sizes of ~22 nm homogeneously distributed within the grains and a few plate-like precipitates, primarily distributed along the grain boundaries, having average lengths of ~50 nm. There were precipitate free zones (PFZ) having widths of ~100 nm lying along the grain boundaries (GB) after post-ECAP annealing at 393 K for 5 h and in Figure 3(a) the SAED pattern along $<112>_{Al}$ shows that the major precipitates in this sample are η' and GP zones but also with the presence of weak spots of Al_3Zr and some T and E phases. Increasing the annealing time leads to more precipitates distributed within the matrix. Thus diffraction along $<111>_{Al}$ in Figure 3(d) shows that the main precipitates homogeneously distributed in the Al matrix after annealing at 393 K for 20 h are primarily η' along $\{011\}_{Al}$, $\{201\}_{Al}$, $\{202\}_{Al}$ and $\{402\}_{Al}$ but some η along $\{110\}_{Al}$ was also detected. The number fractions of fine spherical precipitates with diameter ranges of ~2 to 10 nm and the limited numbers of plate-like precipitates with mean lengths of ~70 nm have both increased by comparison with annealing for 5 h as displayed in Figure 3(a).

Increasing the annealing temperature from 393 to 423 K, as in Figures 3(b) and (e), the PFZ almost disappear. There are now coarser precipitates along the grain boundaries after post ECAP HT at 423 K for 5 h with average lengths of ~ 60 nm and fine spherical precipitates distributed in the matrix with size of ~28 nm. Increasing the annealing time to 20 h gives a minor increase to

~30 nm for the size of the fine spherical precipitates within the matrix together with plate-like precipitates having lengths of ~90 nm as shown in Figure 3(e). The SAED in Figure 3(b) shows that the precipitates are mainly of η' close to $\{202\}_{Al}$ with η along $\{111\}_{Al}$ after annealing for 5 h in Figure 3(b) and with η' along $\{110\}_{Al}$ and η along $\{111\}_{Al}$ after 20 h as in Figure 3(e).

A further increase in the annealing temperature to 473 K leads to average lengths of the plate-like precipitates increasing from ~100 and ~110 nm and average diameters of the spherical precipitates increasing from ~35 nm to ~42 nm after holding from 5 to 20 h. These precipitates are mainly of the η', η, T and E phases as in Figure 3(c) and (f). By comparason with annealing at 393 and 423 K, annealing at 473 increases the precipitate sizes and concurrently decreases the numbers of fine precipiates with a transformation of η' to η. In addition, some T ($Al_{20}Cu_2Mn_3$) and E ($Al_{18}Mg_3Cr_2$) phases were detected showing a plate-like shape and larger than the $MgZn_x$ phase under all processing conditions.

3.3 Microstructures for post-ECAP annealing after 4 and 8 passes

Processing by ECAP produced fairly homogeneous grain structures with average grain sizes of ~200 and ~190 nm and having dislocation densities of 3.20×10^{14} and $3.25 \times 10^{14}\,m^{-2}$ after ECAP through 4 and 8 passes, respectively. In addition, fine η' precipitates with average diameters of ~10 and ~12 nm formed which are uniformly distributed in the matrix together with coarse spherical precipitates having average sizes of ~60 nm and ~65 nm for the 4 and 8 pass samples, respectively[21].

Detailed inspections by TEM of the microstructures of the 4 pass samples after various heat treatments shows that the high dislocation density is maintained and recovery occurrs after annealing at 393 K for 20 h as in Figure 4(a). Increasing the annealing temperature to 423 K for 20 h gives additional recovery as in Figure 4(b). In Figure 4(c) for annealing for 20 h at 473 K,

the mean grain size increases to ~240 nm. This change is relatively small by comparison with the grain size of ~200 nm after ECAP for 4 passes and this is because the precipitates tend to pin the grain boundaries and hinder grain growth [21].

For the 8 pass samples subjected to 5 h anneals, recrystallization is initiated during the post-ECAP anneal at 393 K, continues at 423 K and then becomes complete at 473 K as demonstrated by the clear grains and few intragranular dislocations, as shown in Figures 5(a), (b) and (c). Increasing the annealing time to 20 h for the samples annealed at 393 and 423 K leads to additional clear grains due to further recrystallization and with microstructures. After annealing at 473 K for 5 and 20 h, the grains coarsen slightly from ~220 to ~230 nm as shown in Figures 5(c) and (d).

Figures 6 and 7 show the precipitates in the 4 and 8 pass samples after post-ECAP annealing at 393, 423 and 473 K for 5 and 20 h, respectively. Thus, as the post-ECAP annealing temperature or the annealing time increases, so the sizes of the precipitates increase but their number density decreases. In addition, more η' transforms to η phase. After annealing at 393 and 423 K only limited η phase is visible in the matrix whereas after annealing at 473 K there are large numbers of η precipitates. For convenience, detailed summaries of the precipitate measurements are given in Tables 1 and 2.

3.4 A comparison of all microstructures after post-ECAP annealing for 20 h

Figure 8 displays STEM images after post-ECAP annealing for 20 h showing the influence of the numbers of ECAP passes on the precipitate morphologies. It is important to note initially that the precipitates tend to be distributed uniformly under all of these annealing conditions. After annealing at 393 K (upper row), the microstructures have a small number of larger particles located primarily along the grain boundaries with numerous fine precipitates distributed within

the grains. The average sizes of the fine precipitates were ~8 to ~21 nm while the larger precipitates were ~70 to ~75 nm as shown in Figures 8(a), (b) and (c). The numbers of precipitates were reduced significantly after annealing for 20 h at the higher temperature of 473 K as shown in Figures 8(d), (e) and (f). As the numbers of ECAP passes increased from 1 to 8, the average sizes of these finer precipitates increased from ~42 to ~60 nm while the larger precipitates increased from ~110 to ~140 nm.

4. Discussion

4.1 An evaluation of the experimental results

Close inspection shows there is a general consistency between the hardness measurements and the microstructural observations. In Figure 1 the hardness increases by ECAP processing and the precise value of the hardness increases with increasing numbers of ECAP passes. This hardening is due to a combination of the refining of the grains from ~1.3 μm to ~190 nm, the reduction in the size of the η' precipitates from ~120 to ~12 nm through fragmentation, the formation of more fine precipitates by dissolution and precipitation, and the high density of dislocations produced during ECAP [21-23].

The measured variations in the hardness of the post-ECAP heat treated alloy are attributed to the variations in the matrix grain size and in the effect of different evolutions for the dislocations and precipitates during the post-ECAP heat treatments. It was shown earlier [20] that the alloy after 1 pass of ECAP has a high density of dislocations of ~3.5 × 10^{14} m^{-2}. The present experiments show that this dislocation density decreases only slightly during post-ECAP annealing at 393 K for 5 to 20 h so that a hardening effect remains under these conditions [23]. In addition, annealing at 393 K for 5 h for the 1 pass samples increases the numbers of fine precipitates which are mainly GP zones and η' precipitates. Increasing the annealing time to 20 h

9

leads to a transformation of additional GP zones into ultrafine η' so that there are then additional and finer precipitates of η' with an average size of ~8 nm distributed homogeneously in the matrix. This leads to an increase in hardness which increases with increasing annealing time at 393 K. Annealing at 423 K, with times extending from 5 to 20 h, the advent of recovery decreases the numbers of dislocations and at the same time the size of the η' phase coarsens and their number decreases so that the hardness decreases. After annealing at 473 K for more than 5 h, the sharp decrease in hardness for the 1 pass sample is caused by the occurrence of recrystallization which reduces the dislocation density together with the formation of additional non-coherent η precipitates as shown in Figures 2(c) and (f) and Figures 3(c) and (f).

Annealing the alloy after 8 passes reduces the hardness by comparison with the samples before annealing as shown in Figure 1(c). The precipitates are coarser and more η phase is formed after post-ECAP annealing of the 8 pass sample resulting from the high stored energy which leads to an increase in the diffusive rate of solutes during annealing [26]. In addition, the high stored energy in the sample processed through 8 ECAP passes promotes the occurrence of recrystallization even when annealing at 393 K for 5 h as illustrated in Figure 5(a), and this thereby reduces the hardening through dislocation annihilation.

4.2 Determining the optimum conditions for post-ECAP annealing of an Al-Zn-Mg alloy

When the Al-Zn-Mg alloy is processed by ECAP at 423 K there is a very significant increase in hardness after only 1 pass and further very minor increases in hardness after additional numbers of passes. However, the hardness may be even further increased above the level produced by ECAP through, as documented in Figure 1, giving an additional post-ECAP anneal at 393 K for 20 h. Conversely, there is only a minor additional increase in hardness above the level for ECAP processing when the sample is processed by ECAP for 4 passes and subjected

to an additional anneal at 393 K and there is a significant decrease in hardness when the post-ECAP annealing is conducted after processing by ECAP through 8 passes. In addition, there are consistent losses in hardness due to recrystallization and recovery when the samples are subjected to post-ECAP annealing at 473 K and only minor hardness additions are achieved under some limited conditions when the post-ECAP annealing is at 423 K. These results lead to the conclusion that a post-ECAP anneal is effective for the Al-Zn-Mg alloy only when the numbers of ECAP passes are very small, and certainly no higher than 4 passes, and when the post-ECAP annealing is conducted at a relatively low temperature such as 393 K to avoid grain growth.

The present results are important because it appears that they may conflict with earlier reports of increases in hardness in aluminum-based alloys after post-ECAP annealing treatments. It is appropriate, therefore, to examine these earlier results in more detail.

In the Al-7075 alloy reporting an increase in hardness after a post-ECAP anneal, the alloy was processed by ECAP at 393 K for 3 passes and then annealed at 393 K for 16 h [14]. In the Al-7075 alloy containing Sc, the alloy was processed by ECAP for 1 pass and then annealed at 373 K for 10 or 20 h [18]. Finally, the Al-6061 alloy was processed by ECAP for 4 passes and then annealed at 373 K for 48 h [19]. It is important to note that all of these earlier results are consistent with the present data because the annealing temperatures were consistently lower than 400 K and the processing by ECAP never exceeded a total of 4 passes. It is concluded, therefore, that the use of a post-ECAP annealing treatment is effective in Al-based alloys only when the ECAP processing is conducted to low numbers of passes and the annealing temperature is maintained at a low level.

5. Summary and conclusions

1) ECAP processing effectively hardens an Al-Zn-Mg alloy in the peak aging state. When the numbers of ECAP passes increase from 1 to 8, the hardness increases due to a combination of grain refinement, the formation of large numbers of fine precipitates and the introduction of a high dislocation density.

2) When the ECAP is conducted through only 1 and 4 passes at 423 K, additional hardness may be attained by post-ECAP annealing at 393 K for up to 20 h. No additional hardness may be achieved by post-ECAP annealing when the alloys is initially processed by ECAP through 8 passes and there is only a minor increase in hardness under some limited conditions when the initial processing is conducted through 4 passes.

3) The use of a post-ECAP anneal is only effective in increasing the hardness of the Al-Zn-Mg alloy under very limited conditions when the number of ECAP passes is low (< 4 passes) and the annealing temperature is low (below ~400 K).

Conflict of Interest

The authors declare no conflict of interest.

References

[1] M.E. Fine, *Mater. Trans. A* **1975**, *6A*, 625.

[2] E.A. Starke, J.T. Staley, *Prog. Aerospace Sci.* **1996**, *32*, 131.

[3] J.K. Park, A. J. Ardell, *Mater. Sci. Eng.* **1989**, *A114*, 197.

[4] F. Viana, A.M.P. Pinto, H.M.C. Santos, A.B. Lopes, *J. Mater. Process. Technol.* **1999**, *92-93*, 54.

[5] R. DeIasi, P. N. Adler, *Metall. Mater. Trans. A*, **1977**, *8A*, 1177.

[6] H. Chen, B. Yang, *Mater. Trans.*, **2008**, *49*, 2912.

[7] R.Z.Valiev, R.K.Islamgaliev, I.V.Alexandrov, *Prog. Mater. Sci.* **2000**, *45*, 103.

[8] R.Z. Valiev, T.G. Langdon, *Prog. Mater. Sci.* **2006**, *51*, 881.

[9] R.Z. Valiev, Y. Estrin, Z. Horita, T.G. Langdon, M.J. Zehetbauer, Y.T. Zhu, *JOM* **2006**, *58*(4), 33.

[10] T.G. Langdon, *Acta Mater.* **2013,** *61*, 7035.

[11] R.Z. Valiev, Y. Estrin, Z. Horita, T.G. Langdon, M.J. Zehetbauer, Y. Zhu, *JOM* **2016**, *68*, 1216.

 [12] J. Gubicza, I. Schiller, N.Q. Chinh, J. Illy, Z. Horita, T.G. Langdon, *Mater. Sci. Eng.* **2007**, *A460-461*, 77.

[13] L.J. Zheng, C.Q. Chen, T.T. Zhou, P.Y. Liu, M.G. Zeng, *Mater. Char.* **2002**, *49*, 455.

[14] L.J. Zheng, H.X. Li, M.F. Hashmi, C.Q. Chen, Y. Zhang, M.G. Zeng, *J. Mater. Process. Technol*. **2006**, *171*, 100.

[15] K.R. Cardoso, D.N. Travessa, W.J. Botta, A.M. Jorge, *Mater. Sci. Eng.* **2011**, *A528*, 5804.

[16] M.H. Shaeri, M.T. Salehi, S.H. Seyyedein, M.R. Abutalebi, J.K. Park, *Mater. Des.* **2014**, *57*, 250.

[17] S. R. Kumar, K. Gudimetla, P. Venkatachalam, B. Ravisankar, K. Jayasankar, *Mater. Sci. Eng.* **2012**, *A533*, 50.

[18] W.J. Kim, J.K. Kim, H.K. Kim, J.W. Park, Y.H. Jeong, *J. Alloys Compd.* **2008**, *450*, 222.

[19] J.K. Kim, H.G. Jeong, S.I. Hong, Y.S. Kim, W.J. Kim, *Scripta Mater.* **2001**, *45*, 901.

[20] F.Jiang, L. Tang, J. Huang, Y.Cai, Z.Yin, *Mater. Charact.* **2019**, *153*, 1.

[21] M.A. Afifi, P.H.R. Pereira, Y.C. Wang, Y. Wang, S. Li, T.G. Langdon, *Mater. Sci. Eng.* **2017**, *A684*, 617.

[22] M.A. Afifi, Y.C. Wang, P.H.R. Pereira, Y. Wang, S. Li, Y. Huang, T.G. Langdon, *Mater. Sci. Eng.* **2018**, *A712*, 146.

[23] M.A. Afifi, Y.C. Wang, P.H.R. Pereira, Y. Huang, Y. Wang, X. Cheng, S. Li, T.G. Langdon, *J. Alloys Compd.* **2018**, *749*, 567.

[24] Y. Iwahashi, J. Wang, Z. Horita, M. Nemoto, T.G. Langdon, *Scripta Mater.* **1996**, *35*, 143.

[25] M. Furukawa, Y. Iwahashi, Z. Horita, M. Nemoto, T.G. Langdon, *Mater. Sci. Eng.* **1998**, *A257*, 328.

[26] R.B. Schwarz, *Mater. Sci. Forum* **1998**, *269-272*, 665.

Figure captions

Figure 1. Vickers Microhardenss vs. annealing time curves at different temperatures for the Al-Zn-Mg alloy after post-ECAP annealing for (a) 1 pass, (b) 4 passes and (c) 8 passes.

 F**igure 2**. TEM images of the Al-Zn-Mg alloy after post-ECAP annealing for 1 pass at (a) 393 K, (b) 423 K and (c) 473 K for 5 h and at (d) 393 K, (e) 423 K and (f) 473 K for 20 h.

 Figure 3. TEM images of the Al-Zn-Mg alloy showing precipitate characteristic after post-ECAP annealing for 1 pass at (a) 393 K, (b) 423 K and (c) 473 K for 5 h and at (d) 393 K, (e) 423 K and (f) 473 K for 20 h.

Figure 4. TEM images of the Al-Zn-Mg alloy after post-ECAP annealing for 4 passes at (a) 393K, (b) 423 K and (c) 473 K for 20 h.

Figure 5. TEM images of the Al-Zn-Mg alloy after post-ECAP annealing for 8 passes at (a) 393 K for 5 h, (b) 423 K for 5 h, (c) 473 K for 5 h and (d) 473 K for 20 h.

Figure 6. TEM images of the Al-Zn-Mg alloy showing precipitate characteristic after post-ECAP annealing for 4 passes annealing at (a) 393 K, (b) 423 K, (c) 473 K for 5 h and at (d) 393 K, (e) 423 K, and (f) 473 K for 20 h.
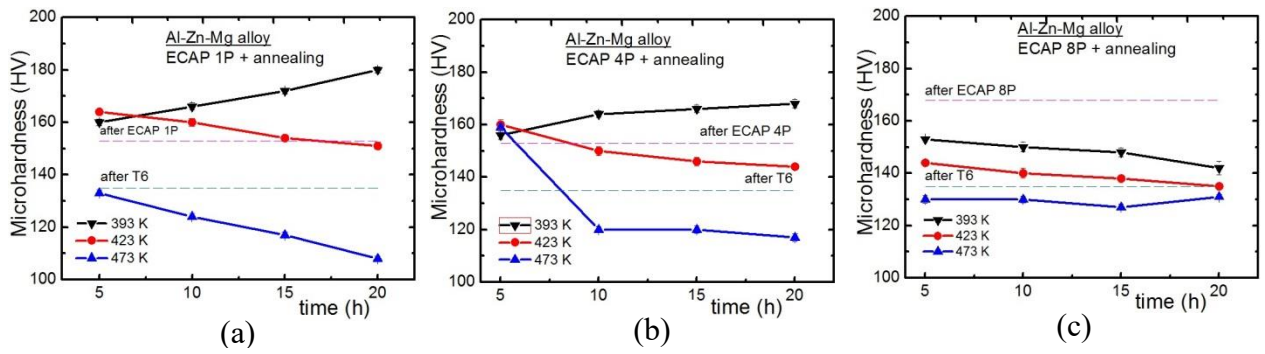
Figure 7. TEM images of the Al-Zn-Mg alloy showing precipitate characteristic after post-ECAP annealing for 8 passes at (a) 393 K, (b) 423 K, (c) 473 K for 5 h and at (d) 393 K, (e) 423 K, (f) 473 K for 20 h.

Figure 8. STEM images of the Al-Zn-Mg alloy showing precipitate characteristic after post-ECAP annealing for (a) 1 pass, (b) 4 passes and (c) 8 passes at 393 K for 20 h and after post-ECAP annealing for (d) 1 pass, (e) 4 passes and (f) 8 passes at 473K for 20 h.
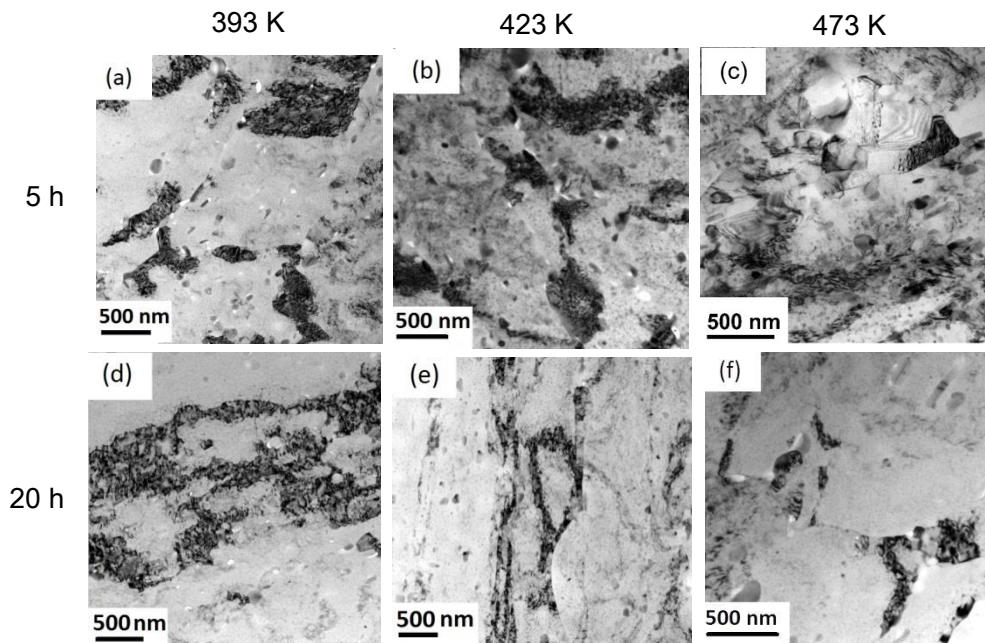
Table 1. Summary of microstructural features in ECAP-processed Al alloy followed by annealing at different temperatures for 5 h.

Table 2. Summary of microstructural features in ECAP-processed Al alloy followed by annealing at different temperatures for 20 h.
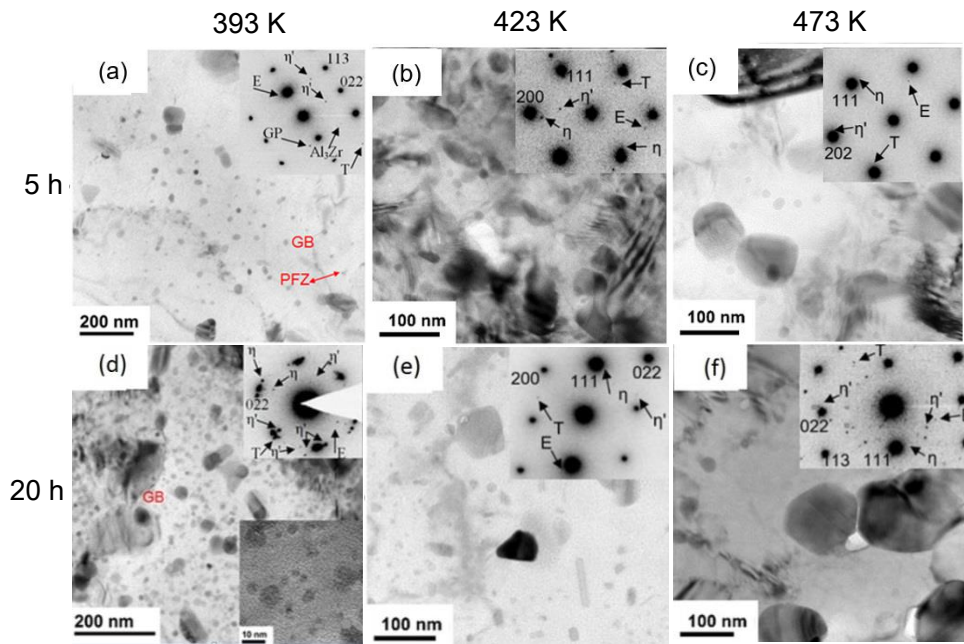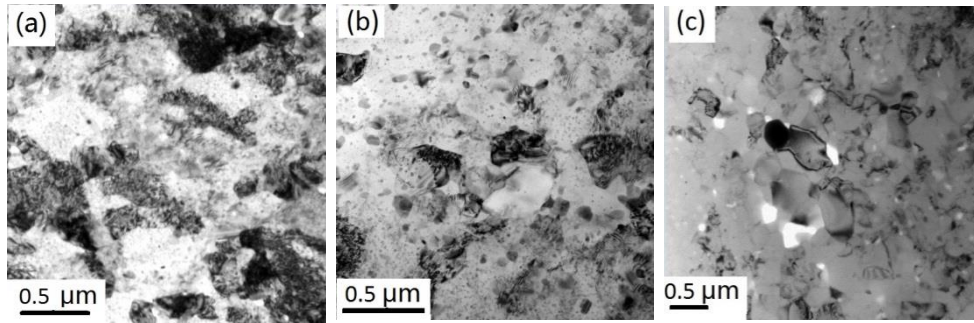
Figure 1. Vickers Microhardenss vs. annealing time curves at different temperatures for the Al-Zn-Mg alloy after post-ECAP annealing for (a) 1 pass, (b) 4 passes and (c) 8 passes.
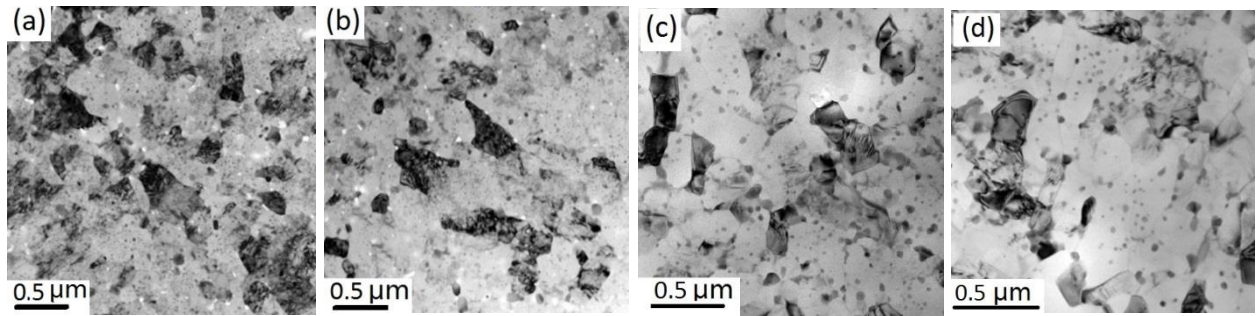
Figure 2. TEM images of the Al-Zn-Mg alloy after post-ECAP annealing for 1 pass at (a) 393 K, (b) 423 K and (c) 473 K for 5 h and at (d) 393 K, (e) 423 K and (f) 473 K for 20 h.
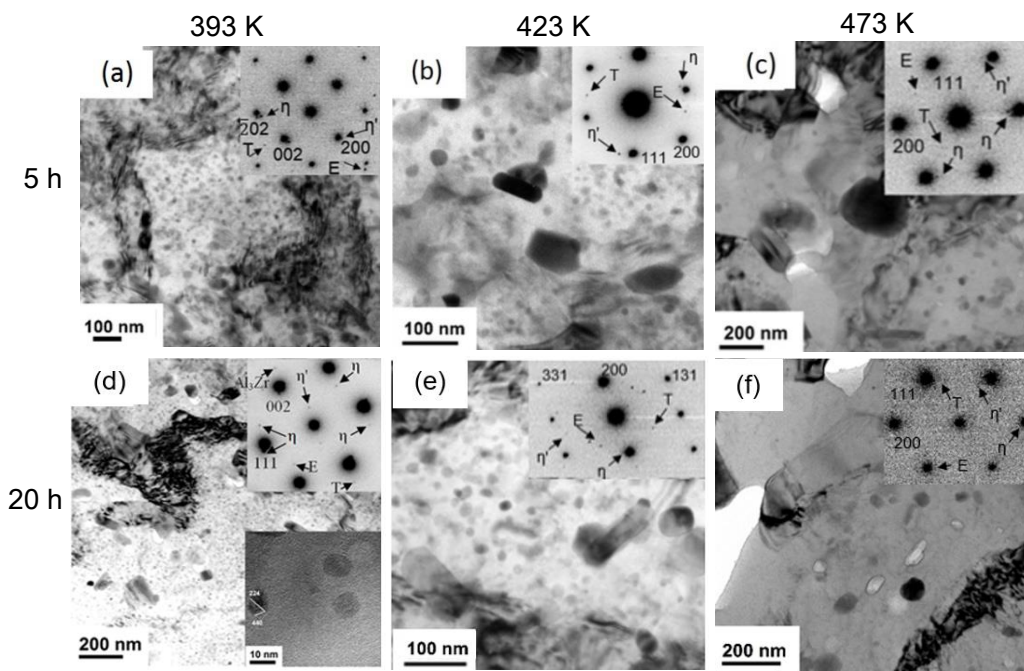
Figure 3. TEM images of the Al-Zn-Mg alloy showing precipitate characteristic after post-ECAP annealing for 1 pass at (a) 393 K, (b) 423 K and (c) 473 K for 5 h and at (d) 393 K, (e) 423 K and (f) 473 K for 20 h.
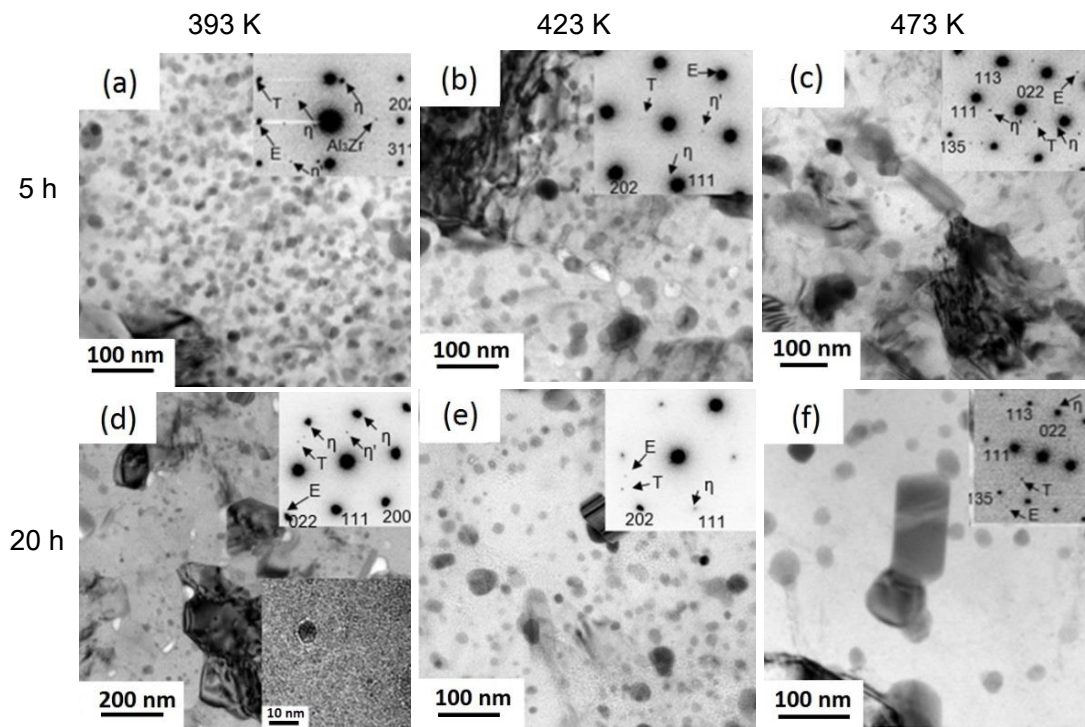
Figure 4. TEM images of the Al-Zn-Mg alloy after post-ECAP annealing for 4 passes at (a) 393K, (b) 423 K and (c) 473 K for 20 h.
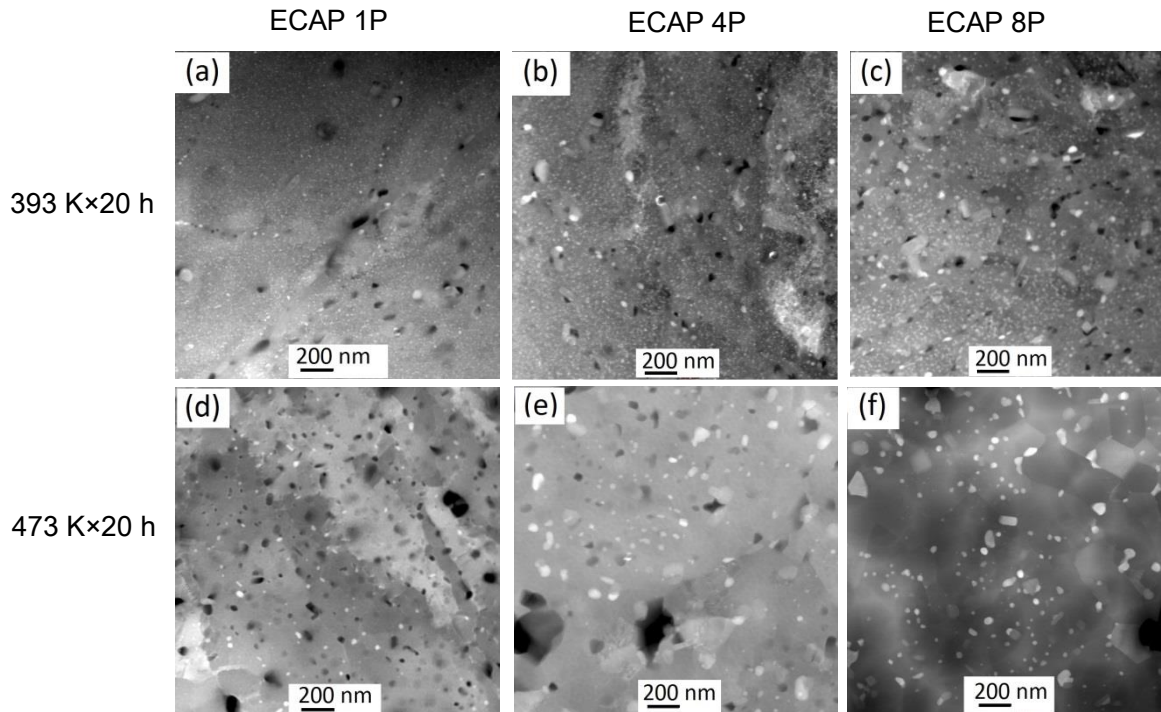
Figure 5. TEM images of the Al-Zn-Mg alloy after post-ECAP annealing for 8 passes at (a) 393 K for 5 h, (b) 423 K for 5 h, (c) 473 K for 5 h and (d) 473 K for 20 h.

Figure 6. TEM images of the Al-Zn-Mg alloy showing precipitate characteristic after post-ECAP annealing for 4 passes annealing at (a) 393 K, (b) 423 K, (c) 473 K for 5 h and at (d) 393 K, (e) 423 K, and (f) 473 K for 20 h.

Figure 7. TEM images of the Al-Zn-Mg alloy showing precipitate characteristic after post-ECAP annealing for 8 passes at (a) 393 K, (b) 423 K, (c) 473 K for 5 h and at (d) 393 K, (e) 423 K, (f) 473 K for 20 h.

Figure 8. STEM images of the Al-Zn-Mg alloy showing precipitate characteristic after post-ECAP annealing for (a) 1 pass, (b) 4 passes and (c) 8 passes at 393 K for 20 h and after post-ECAP annealing for (d) 1 pass, (e) 4 passes and (f) 8 passes at 473K for 20 h.

Table 1. Summary of microstructural features in ECAP-processed Al alloy followed by annealing at different temperatures for 5 h.

	ECAP 1P 5 h			ECAP 4P-5 h			ECAP 8P-5 h		
	393 K	423 K	473 K	393 K	423 K	473 K	393 K	423 K	473 K
Grain size (nm)	870	900	950	210	220	225	200	215	220
Precipitates type (size/nm)	G.P., η', T, E	η', η, T, E	η', η, T, E	G.P., η', η, T, E	η', η, T, E	η', η, T, E	η', η, T, E	η', η, T, E	η', η, T, E
Precipitates size (nm)	D ~22 L~50	D ~28 L~60	D ~35 L~100	D~30	D~37 L~50	D~42 L~75	D~25	D~35	D~40

Table 2. Summary of microstructural features in ECAP-processed Al alloy followed by annealing at different temperatures for 20 h.

	ECAP 1P-20 h			ECAP 4P-20 h			ECAP 8P-20 h		
	393 K	423 K	473 K	393 K	423 K	473 K	393 K	423 K	473 K
Grain size (nm)	900	920	1000	230	230	240	210	220	230
Precipitates type	η', T, E	η', η, T, E	η', η, T, E	η', η, T,E	η', η, T,E	η', η, T,E	η', η, T, E	η', η, T, E	η, T, E
Precipitates size (nm)	D ~8 L~70	D ~30 L~90	D ~42 L~110	D ~14 L~60	D ~40 L~75	D ~50 L~80	D ~21 L~75	D ~45 L~85	D ~60 L~140